Volume 13
Number 18
14 May 2022
Pages 5029–5418

Chemical Science

rsc.li/chemical-science

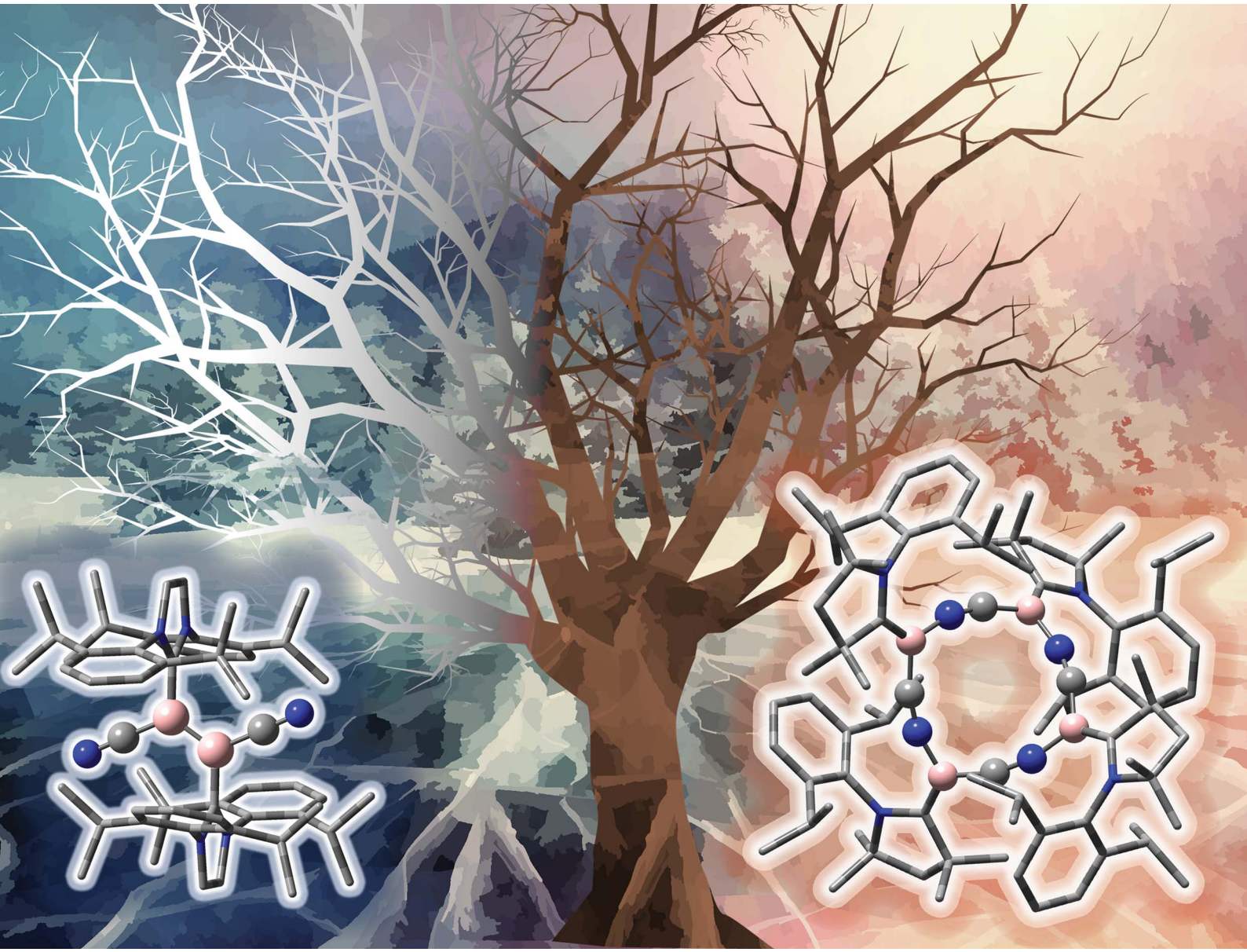

ISSN 2041-6539

ROYAL SOCIETY OF CHEMISTRY

EDGE ARTICLE

Felipe Fantuzzi, Bernd Engels *et al.*
Can a Wanzlick-like equilibrium exist between dicoordinate borylenes and diborenes?

Chemical Science

ROYAL SOCIETY OF CHEMISTRY

EDGE ARTICLE

View Article Online
View Journal | View Issue

Check for updates

Cite this: *Chem. Sci.*, 2022, **13**, 5118

All publication charges for this article have been paid for by the Royal Society of Chemistry

Can a Wanzlick-like equilibrium exist between dicoordinate borylenes and diborenes?†

Felipe Fantuzzi, *[abcd] Yinchun Jiao, [e] Rian D. Dewhurst, [bc] Frank Weinhold, [f] Holger Braunschweig [bc] and Bernd Engels *[a]

Boron chemistry has experienced tremendous progress in the last few decades, resulting in the isolation of a variety of compounds with remarkable electronic structures and properties. Some examples are the singly Lewis-base-stabilised borylenes, wherein boron has a formal oxidation state of +I, and their dimers featuring a boron–boron double bond, namely diborenes. However, no evidence of a Wanzlick-type equilibrium between borylenes and diborenes, which would open a valuable route to the latter compounds, has been found. In this work, we combine DFT, coupled-cluster, multireference methods, and natural bond orbital/natural resonance theory analyses to investigate the electronic, structural, and kinetic factors controlling the reactivity of the transient CAAC-stabilised cyanoborylene, which spontaneously cyclotetramerises into a butterfly-type, twelve-membered $(BCN)_4$ ring, and the reasons why its dimerisation through the boron atoms is hampered. The computations are also extended to the NHC-stabilised borylene counterparts. We reveal that the borylene ground state multiplicity dictates the preference for self-stabilising cyclooligomerisation over boron–boron dimerisation. Our comparison between NHC- *vs.* CAAC-stabilised borylenes provides a convincing rationale for why the reduction of the former always gives diborenes while a range of other products is found for the latter. Our findings provide a theoretical background for the rational design of base-stabilised borylenes, which could pave the way for novel synthetic routes to diborenes or alternatively non-dimerising systems for small-molecule activation.

Received 29th October 2021
Accepted 3rd March 2022

DOI: 10.1039/d1sc05988b

rsc.li/chemical-science

Open Access Article. Published on 04 March 2022. Downloaded on 2/6/2026 3:42:06 PM.
This article is licensed under a Creative Commons Attribution-NonCommercial 3.0 Unported Licence.

Introduction

The Wanzlick equilibrium is a fundamental process whereby two diaminocarbenes, $[(R_2N)_2C:]$, are in equilibrium with their C=C bonded dimers, *i.e.* $[(R_2N)_2C{=}C(NR_2)_2]$ (Scheme 1a).[1] While the Wanzlick equilibrium has only been confirmed to occur with a few specific carbenes, the process is of fundamental and historical interest in persistent carbene chemistry,[2] and has even been observed in higher homologues of carbenes[3] and a dialumene.[4]

Dicoordinate borylenes of the form [LRB:] (L = Lewis base), isolobal and isoelectronic analogues of carbenes $[R_2C:]$, are very rare species. Contrary to their naked borylene analogues [RB:], which exhibit singlet ground states regardless of the R groups,[5] [LRB:] species can have either singlet or triplet ground states.[6] Two examples of dicoordinate borylenes have been isolated by employing π-accepting carbene ligands, the groups of Stephan and Bertrand using a cyclic (alkyl)(amino)carbene (CAAC) (**I**, Scheme 1b),[7] and that of Hudnall using a diamidocarbene (**II**).[8] Beyond isolated examples of dicoordinate borylenes, transient examples (**III–V**, Scheme 1b) have been inferred as intermediates in an intramolecular C–C insertion reaction,[9] transition-metal-like ligand exchange reactions at boron,[10] borylene-mediated dinitrogen fixation and dimerisation,[11] and others.[12] These species can also be generated from the more common doubly base-stabilised $[L^1L^2RB:]$ precursors[13] either by photolytic[10a] or thermal[10b] ligand extrusion processes. However, despite the fact that dicoordinate borylenes [LRB:] and their diborene[14] cousins [LRB=BRL] have now been both isolated and inferred from reactivity, no evidence for a bora-Wanzlick equilibrium has been presented. It is also important to note that the reduction of base-stabilised dihaloorganyl boranes $[LBRX_2]$ most often leads to the diborene [LRB=BRL] when the L unit is a poor π-acceptor, but in contrast, boryl radicals,[15]

[a]*Institute for Physical and Theoretical Chemistry, Julius-Maximilians-Universität Würzburg, Emil-Fischer-Str. 42, 97074 Würzburg, Germany. E-mail: bernd.engels@uni-wuerzburg.de*

[b]*Institute for Inorganic Chemistry, Julius-Maximilians-Universität Würzburg, Am Hubland, 97074 Würzburg, Germany*

[c]*Institute for Sustainable Chemistry & Catalysis with Boron, Julius-Maximilians-Universität Würzburg, Am Hubland, 97074 Würzburg, Germany*

[d]*School of Physical Sciences, Ingram Building, University of Kent, Park Wood Road, Canterbury CT2 7NH, UK. E-mail: f.fantuzzi@kent.ac.uk*

[e]*Key Laboratory of Theoretical Organic Chemistry and Functional Molecules, Hunan University of Science and Technology, Xiangtan 411201, China*

[f]*Theoretical Chemistry Institute and Department of Chemistry, University of Wisconsin–Madison, Madison, WI 53706, USA*

† Electronic supplementary information (ESI) available. See DOI: 10.1039/d1sc05988b

© 2022 The Author(s). Published by the Royal Society of Chemistry

Open Access Article. Published on 04 March 2022. Downloaded on 2/6/2026 3:42:06 PM.
This article is licensed under a Creative Commons Attribution-NonCommercial 3.0 Unported Licence.

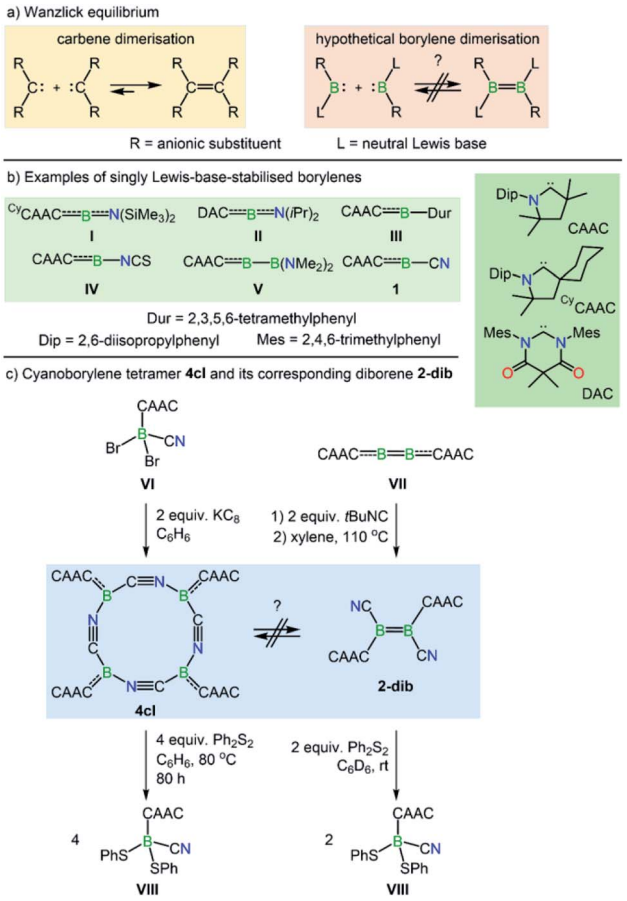

Scheme 1

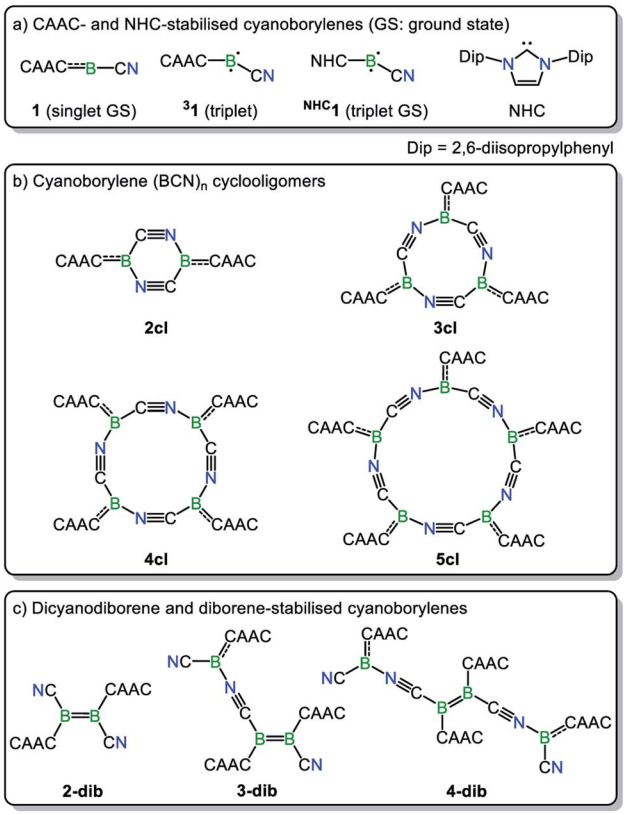

Scheme 2

borylenes, or intramolecular C–C/C–H activation products[16] are formed when the L unit is a strong π-acceptor. The elucidation of the underlying reasons is one of the topics of the present work.

Along these lines, a particularly intriguing case is the singly base-stabilised cyanoborylene [(CAAC)(NC)B:] (**1**, Scheme 1b), which is not known as an isolated species but is present as a constituent fragment in its isolable cyclotetramer (**4cl**, Scheme 1c) and as its B=B-bonded dimer diborene species (**2-dib**, Scheme 1c).[17] Although the borylene cyclotetramer acts as a synthetic equivalent of the cyanoborylene [(CAAC)(NC)B:], and both **4cl** and **2-dib** react with diphenyldisulfide (Ph_2S_2) to afford the CAAC-stabilised borane [(CAAC)B(CN)(SPh)$_2$], no interconversion between the two isomers has been observed.

The close relationship between **4cl** and **2-dib** prompted us to take a closer look into the formation and reactivity of the two species. Considering our experimental findings,[17] a number of questions arise: (i) why does **1** only form **4cl**, but neither **2-dib** nor any smaller (or larger) cyclooligomer? (ii) What is the mechanism of formation of **4cl** from **1**? (iii) Why do **4cl** and **2-dib** form the same product when treated with Ph_2S_2? (iv) Is it possible to form diborene-based oligomers from the reaction of diborenes and borylenes? And, finally, (v) is it possible to tune the cyanoborylene to induce its Wanzlick-like dimerisation through the boron atoms, instead of cyclotetramerisation? To shed some light on these important questions, in this work we performed a thorough computational investigation of the electronic, structural, and reactivity properties of monomeric and oligomeric forms of the CAAC-stabilised cyanoborylene **1** (see Scheme 2) by combining density functional theory (DFT), high-level multireference calculations and natural bond orbital (NBO)[18] analysis. By replacing the CAAC with a classical N-heterocyclic carbene (^{NHC}**1**, see Scheme 2) we also investigate the differences in the electronic structures of the corresponding compounds when a weaker π-accepting and more sterically demanding carbene ligand is used. With this, we will investigate the reasons for the general observation that NHC-stabilised borylenes tend to form diborenes, a trend that is not observed for the CAAC counterparts.[14e]

The nomenclature adopted in our paper is explained in Schemes 1 and 2. The CAAC-stabilised cyanoborylene is abbreviated as **1**, while its corresponding diborene is abbreviated as **2-dib**. Cyclic compounds in which the boron atoms are bridged by CN units are abbreviated as ***n*cl**, in which ***n*** denotes the number of units and **cl** indicates that a closed ring is formed. The corresponding open structures are given as ***n*op**. The prototypical systems formed by the interaction of **1** with **2-dib** are labelled **3-dib** and **4-dib**.

Computational details

First, we benchmarked distinct density functionals against the domain-based local pair natural orbital coupled-cluster theory,

© 2022 The Author(s). Published by the Royal Society of Chemistry

Open Access Article. Published on 04 March 2022. Downloaded on 2/6/2026 3:42:06 PM. This article is licensed under a Creative Commons Attribution-NonCommercial 3.0 Unported Licence.

DLPNO-CCSD(T),[19] for selected closed-shell species and against the multireference N-electron valence state second-order perturbation theory (NEVPT2)[20] approach for open-shell intermediates. The structural properties predicted by the functionals were benchmarked by a comparison with the available X-ray crystal structures. The analysis of the structural data (see Section S1 of the ESI†) indicated that B3LYP[21]-D3(BJ)[22] with Alrich's double-zeta def2-SVP[23] basis set showed the best compromise between accuracy and computational cost, and therefore this combination was used to compute geometries and hessians. Our analysis also showed that ωB97XD[24]/def2-TZVP is more suitable for the relative energies of the closed-shell species, which prompted us to perform additional single-point energy computations at this level for all optimised geometries. All structures were characterised as either minimum energy structures or transition states by the analysis of the vibrational frequencies obtained from the hessian calculations. In order to assess the connectivity between the obtained transition states and the corresponding minimum energy structures, we performed further geometry optimisations along the imaginary mode and additional intrinsic reaction coordinate (IRC)[25] calculations. Free energies were obtained from single-point calculations on the optimised structures at the ωB97XD/def2-TZVP level. Solvation effects were considered using the solvation model for density (SMD)[26] with benzene ($\varepsilon = 2.2706$) as the solvent. A concentration correction of $\Delta G^{0\rightarrow *} = RT\ln(24.46) = 1.89$ kcal mol^{-1} ($T = 298.15$ K) was added to the free energies of all calculated species to change the 1 atm gas-phase values (ΔG^0) to the condensed phase standard state concentration of 1 M (ΔG^*). This leads to a proper description of associative/dissociative steps.[27] For selected cases, we also performed calculations for triplet and open-shell singlet states. These were done using the unrestricted, broken-symmetry DFT approach, as well as with high-level multi-reference calculations based on the complete active space self-consistent field (CASSCF)[28] and NEVPT2 (ref. 20) methods. For these calculations the def2-SVP basis sets was employed. Both approaches, which have been satisfactorily used to describe main-group biradicals and biradicaloids,[29] were used herein to estimate vertical and adiabatic singlet–triplet (S–T) gaps. The biradical character index y_0 was obtained for the open-shell singlet species using the Yamaguchi formula.[30] Finally, the bonding situation of **1** and the ***n*cl** species was investigated with the natural bond orbital (NBO)[18] and natural resonance theory (NRT) methods.[31] All DFT calculations were performed with Gaussian 16, Revision C.01.[32] Multireference calculations were done with Orca 4.1.1,[33] and NBO/NRT calculations were carried out with the NBO 7 program.[34] Images of three-dimensional structures were obtained with CYLview,[35] while molecular orbitals and spin densities were plotted with GaussView 6.0.16.

Results and discussion

Kinetics and thermodynamics of cyclotetramerisation

In this section, we investigate the mechanism of formation of cyanoborylene macrocycles ***n*cl** from the self-stabilising

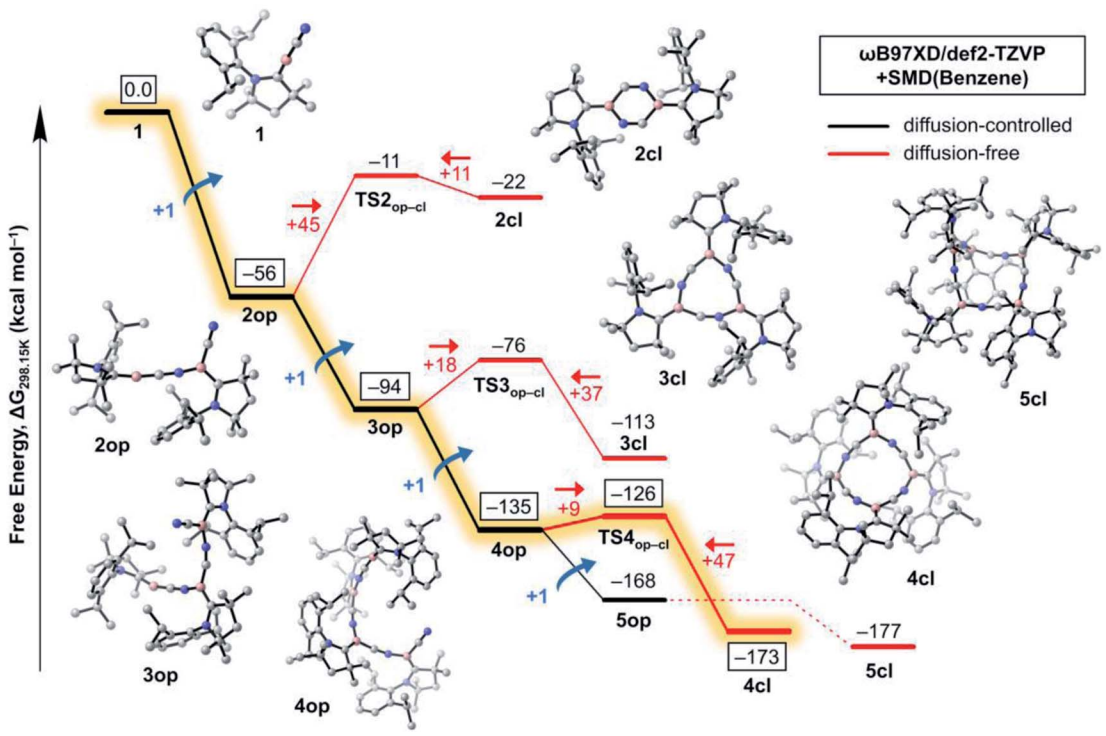

Fig. 1 Free energy profile (ωB97XD/def2-TZVP + SMD(benzene)//B3LYP-D3(BJ)/def2-SVP) of the oligomerisation reaction of **1**. The addition reactions to the open structures are given in black while the cyclomerisations are given in red. Energy barriers for the forward and reverse reactions are also given in red. The most plausible reaction pathway is highlighted in yellow. All ΔG values are given with respect to five non-interacting molecules of **1**.

© 2022 The Author(s). Published by the Royal Society of Chemistry

Open Access Article. Published on 04 March 2022. Downloaded on 2/6/2026 3:42:06 PM.
This article is licensed under a Creative Commons Attribution-NonCommercial 3.0 Unported Licence.

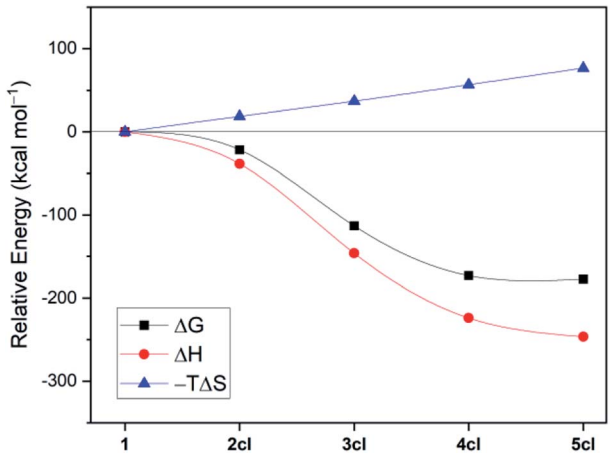

Fig. 2 Disentanglement of the free energies (ωB97XD/def2-TZVP + SMD(benzene)//B3LYP-D3(BJ)/def2-SVP) of cyclooligomerisation of **1** to **2cl**, **3cl**, **4cl**, and **5cl**.

cyclooligomerisation of **1**, aiming at understanding the preference of **4cl** over similar structures. For that purpose, we compute the various possible products of the addition reactions. These structures are given in Scheme 2, and their computed free energies in benzene medium are summarised in Fig. 1–3. In Fig. 1, the addition reactions, which depend on the diffusion-controlled interaction of isolated species, are shown in black, while the intramolecular, diffusion-independent cyclisation reactions are shown in red. The most plausible reaction pathway is highlighted in yellow.

The starting species **1**, which is formed from the reduction of the stable precursor **VI** (see Scheme 1), possesses a singlet ground state with a linear ^{CAAC}C–B–CN arrangement. The lowest triplet state (vertical S–T gap = +14.9 kcal mol^{-1}; adiabatic S–T gap = +5.7 kcal mol^{-1} at the NEVPT2/def2-SVP level) shows a bent structure. The dimerisation of **1** can proceed *via* (i) attachment through the boron atoms, forming the diborene **2-dib**, or (ii) donation from the CN group into the empty p orbital of boron. Reaction through the latter channel will form the open dimer **2op** (see Fig. 1), whose cyclisation leads to the corresponding ring structure **2cl** (see Scheme 2). The formation of **2op** from **1** possesses no reaction barrier (see Fig. S3†), and is strongly exergonic ($\Delta G = -56$ kcal mol^{-1}). The cyclisation leading to the planar **2cl** ring is endergonic by +34 kcal mol^{-1} ($\Delta G = -22$ kcal mol^{-1}), and possesses a high energy barrier of +45 kcal mol^{-1}, as TS2$_{op-cl}$ is located at $\Delta G = -11$ kcal mol^{-1}. The six-membered ring **2cl** is characterised as having a triplet ground state, with a nearby open-shell singlet biradical, whose y_0 is calculated as 0.998 at the CASSCF(6,6)/def2-SVP level of theory (see Fig. S9†), and whose adiabatic S–T gap is merely −0.2 kcal mol^{-1} at the NEVPT2/def2-SVP level. The endergonic character of the cyclisation of **2op** into the open-shell singlet **2cl** is mainly a result of the high ring strain of the latter species, as will be discussed later in more detail.

In contrast to the endergonic cyclisation of **2op**, addition of a third monomeric species **1** leading to **3op** is again very exergonic by −38 kcal mol^{-1}, with **3op** being more stable than three non-interacting molecules of **1** by $\Delta G = -94$ kcal mol^{-1}. Geometry scans following the B–N bond stretch mode (see Fig. S4†) indicate that the formation of **3op** from **2op** is virtually barrierless. Indeed, this was expected as the ***n*op** structures have a bent, terminal B–C–N unit that has the correct orientation to allow the electrophilic attack of the electron-deficient, two-coordinate boron atom of **1** at their terminal CN groups. Subsequent cyclisation to **3cl** is slightly exergonic by −19 kcal mol^{-1}, as **3cl** is located at $\Delta G = -113$ kcal mol^{-1} with respect to **1**. However, an energy barrier of +18 kcal mol^{-1}, less than half of that of **2op** to **2cl**, has to be surmounted, with **TS3$_{op-cl}$** lying at $\Delta G = -76$ kcal mol^{-1}. The free energy variations with respect to the cyclisation of **2op** result from smaller ring strain effects at play in **3cl**. In contrast, the (virtually) barrierless formation of **4op** from **3op** is exergonic by −41 kcal mol^{-1}, indicating that such a transformation is preferred both from a kinetic and thermodynamic perspective, explaining the absence of **3cl** in the experiments.

The structure of **4cl** differs dramatically from those of the smaller cyanoborylene cyclooligomers. The system is composed of a butterfly-shaped, C_2-symmetric twelve-membered ring, whose strain effects are significantly reduced due to loss of planarity. As a consequence, the cyclisation barrier of **4op** to **4cl** is only +9 kcal mol^{-1} and is so exergonic (−38 kcal mol^{-1}) that **4cl** is even lower in energy than **5op** ($\Delta G = -173$ kcal mol^{-1} *vs.* −168 kcal mol^{-1} with respect to **1**). Even with the formation of **5op** being expected to be barrierless due to the reasons discussed above, this pentameric structure will not be formed because its formation is diffusion-controlled, which is kinetically hampered with respect to the diffusion-free, nearly barrierless cyclisation of **4op**. Hence, the butterfly-shaped **4cl** species represents a trap for further oligomerisation, because the formation of **5op** starting from **4cl** has a barrier of about +47 kcal mol^{-1}. This barrier is related to the necessary ring-opening step from **4cl** back to **4op**. In addition, this reaction is slightly endergonic. The cyclopentameric **5cl** species is more

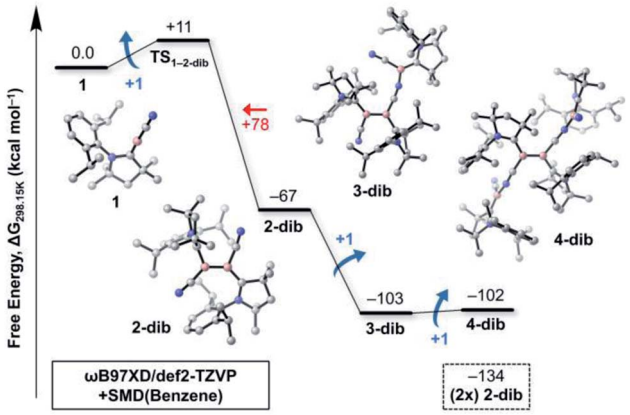

Fig. 3 Free energy profile (ωB97XD/def2-TZVP + SMD(benzene)//B3LYP-D3(BJ)/def2-SVP) of the oligomerisation of **1** to **2-dib** and higher oligomers **3-dib** and **4-dib**. The energy barrier for the dissociation of **2-dib** into two isolated molecules of **1** is given in red. The free energy of formation of two molecules of **2-dib** (−134 kcal mol^{-1}) from isolated **1** units is also shown for comparison.

Open Access Article. Published on 04 March 2022. Downloaded on 2/6/2026 3:42:06 PM. This article is licensed under a Creative Commons Attribution-NonCommercial 3.0 Unported Licence.

stable than **4cl**, but the free energy difference is merely 4 kcal mol^{-1}, indicating the absence of a thermodynamic driving force for ring expansion. Therefore, these results provide strong evidence for the thermodynamic and kinetic preference of **4cl** over its chemically-related analogues, and successfully predict the outcome of the oligomerisation cascade reactions leading to **4cl** from the fleeting CAAC-stabilised cyanoborylene monomer.

Fig. 2 disentangles the enthalpic and entropic contributions to the free energies of formation of the cycles **2cl**, **3cl**, **4cl**, and **5cl**. The ring expansion is both exothermic and exergonic up to **4cl**. As expected, formation of **5cl** from **4cl** is still exothermic, but the entropy contribution (which increases linearly from **2cl** to **5cl** and is particularly destabilising in the latter) flattens the free energy curve. These results reinforce the findings of Fig. 1, revealing that enthalpic and entropic factors contribute to the preferred formation of **4cl** over its analogous cyclooligomers.

While Fig. 1 explains why **4cl** – and not smaller or larger cyanoborylene cyclooligomers – are formed, the question of why two monomers **1** do not form **2-dib** remains open. Additionally the question of why **2-dib** – obtained from the diboryne precursor **VII** (ref. 36) – does not form **4cl** *via* its fragmentation to **1** also arises. These questions are answered in Fig. 3. The formation of **2-dib** from two monomers **1** is as exergonic as the formation of **2op** (see Fig. 1), but for this dimerisation reaction, we predict a reaction barrier of +11 kcal mol^{-1}. Since the formation of **2op** is computed to be barrierless, **1** will only react to **2op**, as this intermediate is kinetically preferred. The difference between the kinetic profile of these dimerisation reactions arises because the formation of **2-dib** requires the distortion of two linear ^{CAAC}C–B–CN units, while for forming **2op** one unit remains linear. The strong exergonicity of the formation of **2-dib** from **1** also explains why the former does not fragment into two monomeric units of **1**, which would be necessary for the interconversion of **2-dib** to the tetramer **4cl**.

The energetic profile of the computed oligomerisation steps strongly suggests that the addition of **1** to **2-dib** should also be exergonic. Indeed, our computations predict that the formation of **3-dib** from **2-dib** is strongly exergonic ($\Delta G = -36$ kcal mol^{-1}). Species **3-dib** can be rationalised as a diborene-stabilised borylene, and, if synthetically achieved, would be the first of its kind. Conversely, the attachment of another borylene to **3-dib**, leading to the diborene-bridged bisborylene **4-dib**, is slightly endergonic and significantly less stable than the formation of two isolated dicyanodiborenes **2-dib** (**4-dib**: $\Delta G = -102$ kcal mol^{-1}; (2×) **2-dib**: $\Delta G = -134$ kcal mol^{-1}). We predict that **3-dib**, a closed-shell singlet molecule with a vertical S–T gap of *ca.* 10 kcal mol^{-1} as predicted by DFT calculations, could be formed by a controlled reaction where small amounts of the cyanoborylene **1** are generated in the presence of an excess of **2-dib**. This would avoid the self-stabilising cyclotetramerisation of **1** to form **4cl**, which is the preferred reaction pathway.

Bonding situation in (BCN)$_n$ cyclooligomers

In order to derive salient information about the bonding situation of the (BCN)$_n$ cyclooligomers, we performed further calculations based on the NBO/NRT approach. Due to size limitations, these calculations were done for model systems where the methyl and Dip groups of the CAAC ligands are replaced by hydrogen atoms. The NRT bond orders of the ^{CAAC}C–B bond and the intraannular B–C, C–N and N–B bonds are shown in Table 1. The values of the most relevant NBO second-order perturbation energies, $E^{(2)}$, associated with the natural resonance structure of largest weight, are shown in Table 2. For the ***n*cl** species (n = 3–5), these values correspond to mean energies $\langle E^{(2)} \rangle$ of the n individual donor–acceptor interactions. The corresponding values of the monomeric cyanoborylene **1** are also shown for comparison.

Table 1 Selected NRT bond orders (^{CAAC}C–B and the intraannular B–C, C–N, and N–B bonds) of **1** and the cyclooligomers **2cl**, **3cl**, **4cl**, and **5cl**, calculated at the (U)B3LYP/def2-SVP level of theory. For the **ncl** species, the values correspond to mean bond orders of the n individual X–Y bonds

	^{CAAC}C–B	B–C	C–N	N–B
1	1.67	1.34	2.62	—
2cl	1.38	1.25	2.41	1.18
3cl	1.49	1.18	2.67	1.13
4cl	1.58	1.17	2.73	1.06
5cl	1.59	1.18	2.75	1.06

The NRT bond order of ^{CAAC}C–B in **1** is 1.68 (see Table 1), indicating a strong backdonation from the boron atom to the CAAC ligand. From the NBO point of view, this interaction is stabilised mainly by a donor–acceptor contribution involving the ^{CAAC}N(lp) donor orbital and the antibonding ^{CAAC}C–B(π^*) acceptor (see Table 2), where the $E^{(2)}$ value is 35.3 kcal mol^{-1}. Analogously, two donor–acceptor pairs of the ^{CAAC}C–B(π) → C–N(π^*) type are found, depending on the orbitals' relative orientation. The first pair is formed between the ^{CAAC}C–B(π) and the C–N(π^*) orbital (quasi-) parallel to it (labelled ^{CAAC}C–B(π) → C–N(π^*)$_{\parallel}$), while the second involves the ^{CAAC}C–B(π) and the (quasi-) perpendicular C–N(π^*) orbital (^{CAAC}C–B(π) → C–N(π^*)$_{\perp}$ term). The sum of these two contributions correspond to the ^{CAAC}C–B(π) → C–N(π^*) values in Table 1 while the individual ^{CAAC}C–B(π) → C–N(π^*)$_{\parallel}$ and ^{CAAC}C–B(π) → C–N(π^*)$_{\perp}$ pairs for **1**, **2cl**, and **4cl** are shown in Fig. 4. In the case of

Table 2 Most relevant NBO second-order perturbation energies $E^{(2)}$ of **1** and the cyclooligomers **2cl**, **3cl**, **4cl**, and **5cl**. For the **ncl** species, the values correspond to mean energies $\langle E^{(2)} \rangle$ of the n individual donor–acceptor interactions. For C–B(π) → C–N(π^*) and, analogously, for C–B(π) → N–C(π^*), contributions coming from the (quasi-)parallel C–B(π) → C–N(π^*)$_{\parallel}$ and (quasi-)perpendicular C–B(π) → C–N(π^*)$_{\perp}$ bonding pairs are considered. See ESI for more details

	^{CAAC}C–B(π) → C–N(π^*)	^{CAAC}C–B(π) → N–C(π^*)	^{CAAC}N(lp) → ^{CAAC}C–B(π^*)
1	24.5	—	35.3
2cl	18.9	11.1	30.3
3cl	28.5	15.0	32.7
4cl	30.6	16.5	34.2
5cl	29.4	17.1	33.1

© 2022 The Author(s). Published by the Royal Society of Chemistry

Open Access Article. Published on 04 March 2022. Downloaded on 2/6/2026 3:42:06 PM.
This article is licensed under a Creative Commons Attribution-NonCommercial 3.0 Unported Licence.

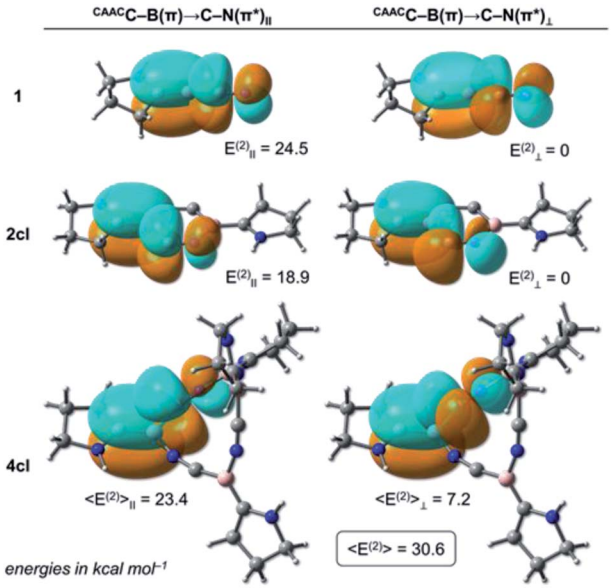

Fig. 4 (Quasi-)parallel (left) and (quasi-)perpendicular (right) ^{CAAC}C–B(π) → C–N(π*) donor–acceptor orbitals of **1** (top), **2cl** (middle) and **4cl** (bottom). Their corresponding second-order perturbation energies $\langle E^{(2)}\rangle_{\parallel}$ and $\langle E^{(2)}\rangle_{\perp}$ are also shown in kcal mol^{-1}. The sum of these two contributions gives $\langle E^{(2)}\rangle$, which for **4cl** is 30.6 kcal mol^{-1}. Level of theory: B3LYP/def2-SVP.

1, the value of ^{CAAC}C–B(π) → C–N(π*)$_{\perp}$ is negligible, with only the parallelly oriented pair contributing to the 24.5 kcal mol^{-1} of the ^{CAAC}C–B(π) → C–N(π*) interaction. The C–N bond order of **1** is 2.62.

Formation of the cyclodimer **2cl**, whose six-membered $(BCN)_2$ ring is fully planar, hampers the ^{CAAC}C–B(π) → C–N(π*) and ^{CAAC}N(lp) → ^{CAAC}C–B(π*) interactions by *ca.* 5 kcal mol^{-1} each. This is followed by a bond order decrease of the ^{CAAC}C–B and the C–N bonds, respectively, to 1.38 and 2.41. Indeed, the NRT and NBO values experience the largest variation in going from **1** to **2cl**, in comparison to those of the subsequent expansions. This is explained by the significant change in the ^{CAAC}C–B–C–N bonding motif, particularly the BCN bond angle, which is 180° in **1** but is compressed to 129° in **2cl**. Such a dramatic structural modification significantly distorts the B–C–N moiety from a perfectly linear arrangement, which leads to a highly strained ring, and reduces the overlap between the ^{CAAC}C–B(π) and C–N(π*) orbital pairs, producing a smaller $E^{(2)}$ contribution. The destabilising nature of the bent B–C–N moiety is also reflected in the electronic structure of **2cl**, whose lowest singlet state has a biradical character, with its corresponding closed-shell singlet lying 6.2 kcal mol^{-1} above at the DFT level. It is important to note that for the cyclic structures each ^{CAAC}C–B(π) donor can interact with a second set of antibonding C–N(π*) acceptors through the B–N–C moiety. These interactions follow similar trends to those through the B–C–N motif, but with smaller energy values.

Inspection of Tables 1 and 2 reveals that the NRT and $E^{(2)}$ values change systematically as the ring size is increased to **4cl**, and then do not vary considerably from **4cl** to **5cl**. For example, the ^{CAAC}C–B bond order of **3cl** (1.49) is larger than that of **2cl** (1.38), but smaller than those of **4cl** (1.58) and **5cl** (1.59), which are virtually identical. Similar trends are observed for the other bonding descriptors. Indeed, **4cl** is the first non-planar $(BCN)_n$ ring, with the adopted butterfly structure significantly decreasing strain effects, and also allowing more interactions due to reduction of symmetry. These findings indicate that **4cl** already possesses the most relevant electronic and structural features contributing to the stabilisation of these $(BCN)_n$ rings, and that further ring expansion does not provide any additional benefit to the system. This is in total agreement with the computational findings based on the thermochemical analysis, which indicate that the thermodynamic driving force for ring expansion is significant only up to **4cl**.

One last point should be noticed in the NBO/NRT values of Tables 1 and 2. The C–N bond orders of **4cl** and **5cl** are significantly larger than that of **1**, with these cyclic systems also featuring larger ^{CAAC}C–B(π) → C–N(π*) $E^{(2)}$ values. The increase of these donor–acceptor contributions comes from the interplay of the ^{CAAC}C–B(π) → C–N(π*)$_{II}$ and ^{CAAC}C–B(π) → C–N(π*)$_{\perp}$ terms as the $(BCN)_n$ rings become non-planar. Due to an orientation mismatch between the (quasi-)parallel ^{CAAC}C–B(π) and C–N(π*) orbitals, the ^{CAAC}C–B(π) → C–N(π*)$_{II}$ $E^{(2)}$ values are slightly decreased to 23.4 and 23.7 kcal mol^{-1}. On the other hand, the ^{CAAC}C–B(π) → C–N(π*)$_{\perp}$ term, which features the (quasi-)perpendicular orbital orientation and is negligible in **1** since these orbitals are perfectly orthogonal, contributes to 7.2 and 5.7 kcal mol^{-1} in **4cl** and **5cl**, respectively. The increase of $E^{(2)}$ due to the (quasi-)perpendicular pair overcompensates the $E^{(2)}$ decrease due to the (quasi-)parallel pair, making the ^{CAAC}C–B(π) → C–N(π*) donor–acceptor contribution more important for the non-planar $(BCN)_n$ rings. Therefore, we can conclude that donor–acceptor contributions of the ^{CAAC}C–B(π) → C–N(π*) type are also at play in the further stabilisation of the non-planar $(BCN)_n$ rings in comparison to their planar analogues.

Thermochemistry of the reaction with Ph_2S_2

At this point, it is very clear that the formation of the **4cl** butterfly cyclotetramer from the cyanoborylene **1** is both thermodynamically and kinetically preferred over the formation of diborene **2-dib**, and that the interconversion of **2-dib** and **4cl** is hampered due to the high B–B dissociation energy of **2-dib**. However, experimental results have shown that these two species have very similar reactivity patterns. In this section, we focus on the reaction of **2-dib** and **4cl** with Ph_2S_2 (see Scheme 1) to shed some light on their reactivity patterns. In both cases, compound **VIII** is formed. The relative free energies of the mentioned species – together with those of plausible intermediate candidates – are shown in Fig. 5.

Addition of Ph_2S_2 across the B–B bond of **2-dib** leads to **Int-1**, where the S–S σ and the B–B π bonds are broken, and two B–S σ bonds are formed. This transformation is slightly endergonic by +3 kcal mol^{-1}. Contrary to **2-dib**, the B–B dissociation of **Int-1**, which leads to two **[Int-2]**$^{\cdot}$ radicals, is exergonic by −28 kcal mol^{-1}. Moreover, reaction with a second Ph_2S_2 compound to form the product **VIII** is also exergonic, with the

Open Access Article. Published on 04 March 2022. Downloaded on 2/6/2026 3:42:06 PM.
This article is licensed under a Creative Commons Attribution-NonCommercial 3.0 Unported Licence.

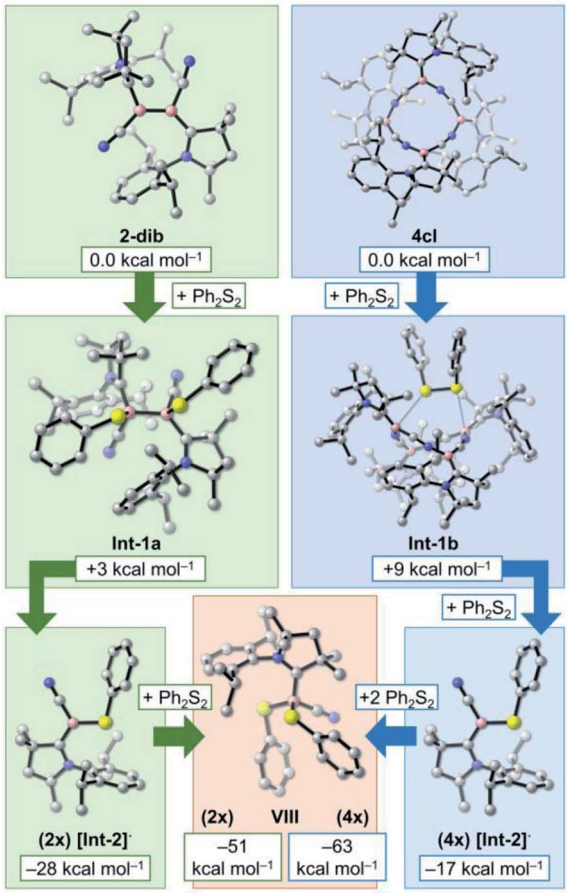

Fig. 5 Computed relative free energies (ωB97XD/def2-TZVP + SMD(benzene)//B3LYP-D3(BJ)/def2-SVP) of **2-dib**, **4cl**, **VIII**, and plausible intermediate candidates for the conversion of **2-dib** and **4cl** into **VIII**. The free energies are obtained from ωB97XD/def2-TZVP + SMD(benzene) single-point calculations of the optimised geometries at the B3LYP-D3(BJ)/def2-SVP level. The values are referenced to the energy of four isolated cyanoborylene molecules **1**.

product located −51 kcal mol^{-1} below **2-dib**. A strong thermodynamic driving force is, therefore, obtained for the chemical transformation of **2-dib** to **VIII**.

In turn, addition of Ph_2S_2 to **4cl** leads to **Int-1b**, which is merely +9 kcal mol^{-1} uphill. Surprisingly, even with **4cl** being very thermodynamically stable, its dissociation into four **[Int-2]**· radicals after insertion of two equivalents of Ph_2S_2 is exergonic. As in the case of **2-dib**, the formation of **VIII** from **4cl** is remarkably favourable. Although the current computations do not unveil the whole mechanistic pathway, they suggest that **4cl** and **2-dib** can have the same reaction outcome even though they are not interconvertible, in accordance with the experimental findings.[17c]

NHC-stabilised cyanoborylenes

While CAAC-stabilized borylenes lead to quite different products, their NHC counterparts tend to form diborenes.[14e] To determine the reasons for this, in this section we investigate the effects that distinct types of carbenes confer on the electronic

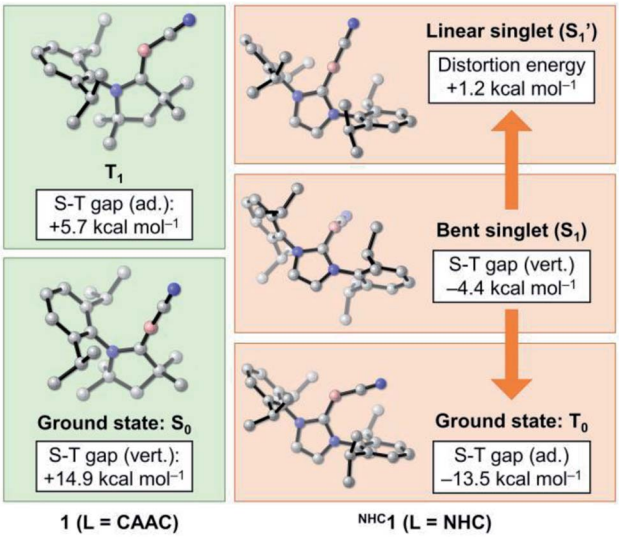

Fig. 6 Energetic and structural features of the ground state and low-lying states of **1** and ^{NHC}**1**. Energies are at the NEVPT2/CASSCF(2,2)/def2-SVP level of theory.

and structural properties of Lewis-base-stabilised cyanoborylene species. For this purpose, the main electrostructural features of the ground states and low-lying states of **1** and ^{NHC}**1**, the latter obtained by replacing the CAAC ligand with the classic imidazolylidene NHC with Dip substituents at the nitrogen atoms, are shown in Fig. 6. The propensity of CAACs to form stable radical and biradical main-group species is now well established, while their NHC analogues more often lead to closed-shell singlet species.[29a,i] However, in the cyanoborylene molecule, this tendency is inverted, as revealed by DFT and, particularly, high-level NEVPT2/CASSCF calculations (Fig. 6). The ground state of the CAAC-stabilised cyanoborylene **1** is a closed-shell singlet system ($\mathbf{S_0}$) featuring a linear ^{CAAC}C–B–CN motif. The vertical excitation to the lowest triplet state ($\mathbf{T_1}$) is +14.9 kcal mol^{-1}. Geometry optimisation at the $\mathbf{T_1}$ potential energy surface leads to a structure having a bent ^{CAAC}C–B–CN moiety oriented parallel to the CAAC ligand, and which lies +5.7 kcal mol^{-1} above that of the $\mathbf{S_0}$ state of **1**. In contrast, the most stable closed-shell singlet ($\mathbf{S_1}$) structure of ^{NHC}**1** features a bent ^{NHC}C–B–CN motif perpendicularly oriented with respect to the NHC plane. The vertical singlet–triplet gap at the NEVPT2 level reveals that the triplet state (T_0) is lower in energy than the singlet with this structure by −4.4 kcal mol^{-1}. Geometry optimisation of the $\mathbf{T_0}$ state of ^{NHC}**1** leads to a structure where the bent ^{NHC}C–B–CN motif is parallelly oriented with respect to the NHC ring, in a similar manner to that of the $\mathbf{T_1}$ structure of **1**. The optimised $\mathbf{T_0}$ state lies −13.5 kcal mol^{-1} below the optimised $\mathbf{S_1}$ state. Finally, a constrained optimisation of the closed-shell singlet ^{NHC}**1**, where the ^{NHC}C–B–C and B–C–N angles are fixed to 180°, therefore producing a linear ^{NHC}C–B–C–N motif, leads to $\mathbf{S_1}'$, which lies +1.2 kcal mol^{-1} above $\mathbf{S_1}$ and +14.7 kcal mol^{-1} above $\mathbf{T_0}$.

In order to shed some light on the destabilising nature of the linear ^{NHC}C–B–CN arrangement in the NHC-stabilised cyanoborylene ^{NHC}**1**, Fig. 7 presents the frontier MOs of the closed-

© 2022 The Author(s). Published by the Royal Society of Chemistry

Open Access Article. Published on 04 March 2022. Downloaded on 2/6/2026 3:42:06 PM.
This article is licensed under a Creative Commons Attribution-NonCommercial 3.0 Unported Licence.

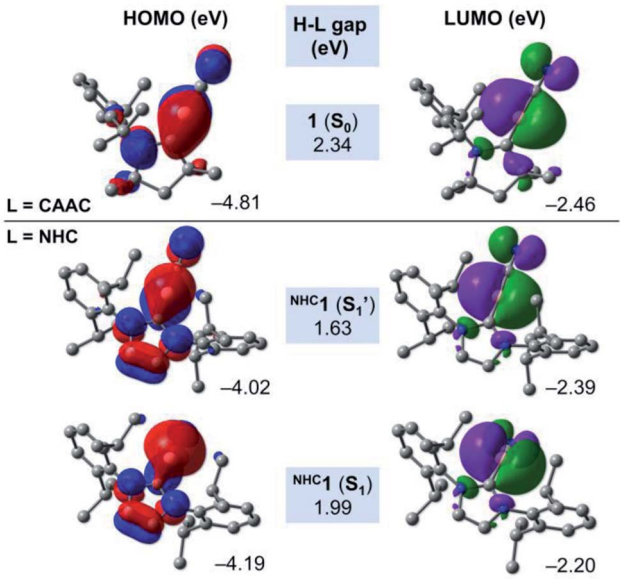

Fig. 7 Canonical Kohn–Sham frontier orbitals and H–L gaps of **1** (S_0), ^{NHC}**1** (S_1) and ^{NHC}**1** (S_1') at the B3LYP-D3(BJ)/def2-SVP level of theory.

shell systems **1** (L = CAAC) and the S_1 and S_1' states of ^{NHC}**1**. The HOMO of **1** (−4.81 eV) is composed of a ^{CAAC}C–B π bonding contribution, which originates from the backdonation of the borylene lone pair to the π acceptor ^{CAAC}C atom. This orbital also features two nodal planes: one in the ^{CAAC}N–^{CAAC}C bonding region, and another in the vicinity of the C–N bond. In turn, the LUMO of **1** (−2.46 eV) is also located in the vicinity of the ^{CAAC}C–B–CN unit, but is orthogonally aligned with respect to the HOMO. This orbital also features antibonding character at the C–N bond, and antibonding σ contributions at the carbene backbone. The HOMO–LUMO (H–L) gap of the S_0 state of **1** is calculated to be 2.34 eV. The replacement of the CAAC ligand by an NHC does not significantly affect either the shape or the orbital energies of the corresponding LUMO orbitals. However, important changes are observed in the HOMOs of the S_1' and S_1 states of ^{NHC}**1**. Both orbitals are characterised by the presence of two nodal planes in the carbene ring. By comparing ^{NHC}**1** (S_1') and **1** (S_0), it is possible to see that the extension of the B → ^{NHC}C backdonation is reduced drastically. This is a direct consequence of the differences in π acidity of the CAAC and NHC ligands. Because of the lower π acidity of the NHC, the HOMO energy of ^{NHC}**1** (S_1') is lifted by around 0.8 eV, consequently decreasing the H–L gap to 1.63 eV. The linear ^{NHC}C–B–CN configuration forces the boron atom to retain its sp hybridisation, which is destabilised due to the smaller backdonation effect. In turn, geometry relaxation of the closed-shell ^{NHC}**1** (S_1) system leads to a bent ^{NHC}C–B–CN moiety perpendicularly aligned with respect to the NHC. This allows the boron atom to change its hybridisation mode to sp^2, with a pure lone pair localised at the boron centre. Compared to ^{NHC}**1** (S_1'), the HOMO of ^{NHC}**1** (S_1) is stabilised by *ca.* 0.2 eV, while the LUMO is lifted to −2.20 eV, leading to a H–L gap value of 1.99 eV. The variations in the H–L gaps are consistent with the energetic features depicted in Fig. 6. They reveal that the smaller π accepting nature of the classical NHC in comparison to that of CAAC, as a consequence of the extra π-donating and σ-withdrawing amino group, is responsible for the destabilisation of the closed-shell NHC analogue of **1**.

In order to investigate in more detail the origin of the preferred bent C–B–CN geometry of ^{NHC}**1** in contrast to the linear arrangement of **1** (L = CAAC), we performed further computations based on the energy decomposition analysis coupled with natural orbitals for chemical valence (EDA-NOCV).[37] These calculations were done for **1** and the corresponding linear singlet (S_1') of ^{NHC}**1** considering the singlet fragments BCN + L = CAAC, NHC at the PBE0 (ref. 38)-D3(BJ)/TZ2P level of theory using the ADF 2019 (ref. 39) program package. It is important to mention that the BCN fragment must be computed in its electronically excited configuration, so that the p(π) lone pair at boron is doubly occupied.[13b] In the EDA-NOCV approach, the interaction energy ΔE_{int} between the fragments is decomposed into distinct contributions, namely Pauli repulsion (ΔE_{pauli}), dispersion (ΔE_{disp}), electrostatic (ΔE_{elstat}) and orbital interaction (ΔE_{orb}) energies. The latter term can be further decomposed into pairwise, donor–acceptor NOCV contributions. The main deformation densities associated with the EDA-NOCV description of **1** and ^{NHC}**1** (S_1') are shown in Fig. 8. All energy terms from the EDA-NOCV decomposition of the aforementioned systems are shown in Table S11† in the ESI.

For **1**, the ΔE_{int} term is computed to be −242.3 kcal mol^{-1}. The Pauli repulsion destabilises this interaction by +142.7 kcal mol^{-1}, which is counterbalanced by the stabilising

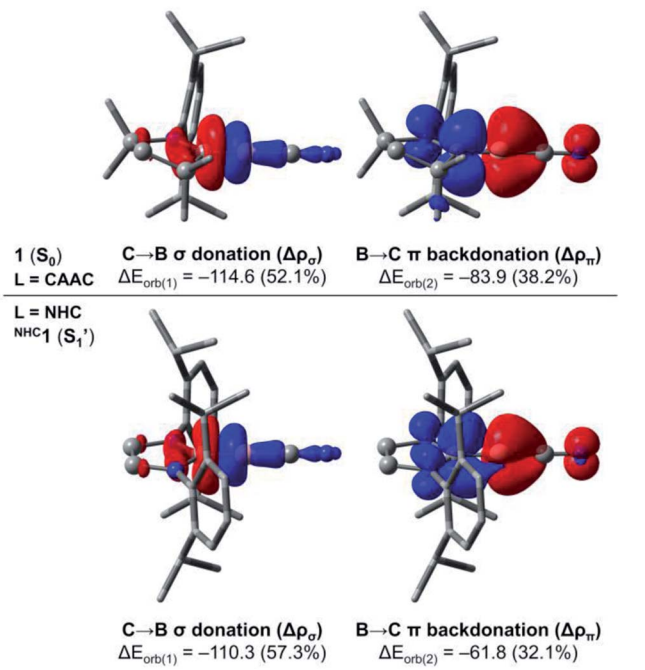

Fig. 8 NOCV deformation densities evidencing the C → B σ donation and the B → C π backdonation in **1** and ^{NHC}**1** (S_1'). Isosurface: 0.003. Charge flows from red to blue. Energies are in kcal mol^{-1}. Level of theory: PBE0-D3(BJ)/TZ2P.

Open Access Article. Published on 04 March 2022. Downloaded on 2/6/2026 3:42:06 PM. This article is licensed under a Creative Commons Attribution-NonCommercial 3.0 Unported Licence.

contributions of the remaining energy terms. While dispersion effects contribute to merely −4.4 kcal mol^{-1}, the ΔE_{elstat} and ΔE_{orb} represent 41.7% (−160.7 kcal mol^{-1}) and 57.1% (−219.9 kcal mol^{-1}) of the stabilising contributions, respectively. A further inspection of the ΔE_{orb} terms reveals that the two major contributions sum to roughly 90% of the total orbital interaction. These contributions are related to C → B σ donation (−114.6 kcal mol^{-1}) and B → C π backdonation (−83.9 kcal mol^{-1}). On the other hand, the EDA-NOCV description of ^{NHC}**1** (**S$_1$′**) indicates that the ΔE_{int} term is −211.5 kcal mol^{-1}, which is 30.8 kcal mol^{-1} less negative than that of **1**. Inspection of the energy terms that compose ΔE_{int} reveals that this difference is mainly attributed to ΔE_{orb}, whose stabilising contributions in ^{NHC}**1** (**S$_1$′**) are smaller by 27.6 kcal mol^{-1}. The analysis of the NOCV pairs clearly indicates that the decrease in the B → C π backdonation is the effect responsible for the less stabilising interaction between the NHC and the linear BCN fragment. In other words, the EDA-NOCV results confirm that the π-acidity of the ligand dictates the preferred linear structure of the CAAC-stabilised borylene, as the B → NHC π backdonation is significantly less effective.

The findings discussed above seem to be of great importance to the chemistry of the borylenes. They strongly suggest that the HOMO–LUMO gap, and consequently the ground state multiplicity, is more dependent on the Lewis base, rather than the R substituent. In that sense, NHC-stabilised borylenes would prefer to form triplet compounds, while their CAAC analogues would form closed-shell singlet species. This preference would lead to distinct reactivity patterns, and could explain the general observation that NHC-stabilised borylenes tend to form diborenes, formally the dimerisation product of triplet borylenes, while those with CAAC donors do not dimerise through the boron atom and show small molecule activation behavior.[14e] To further test this hypothesis, we computed the CAAC- and NHC-stabilised parent borylenes [LHB:] (see Fig. S5 and 6†). Indeed, the structural and electronic properties of [LHB:] are strikingly similar to those of the corresponding cyano compounds **1** and ^{NHC}**1**. While (CAAC)BH presents a linear ^{CAAC}C–B–H bonding motif and a closed-shell singlet ground state, with an S–T gap of +11.0 kcal mol^{-1} at the NEVPT2 level, (NHC)BH has a bent ^{NHC}C–B–H structure with a triplet ground state (S–T gap of −12.0 kcal mol^{-1}). Further calculations to test the generality of these findings to other Lewis-base-stabilised borylenes are in progress.

Lastly, we have analysed the formation of the dicyanodiborene compound stabilised by two NHC ligands, ^{NHC}**2-dib**, from the dimerisation of two cyanoborylenes ^{NHC}**1**. As discussed above, the monomeric structure has a bent ^{NHC}C–B–CN motif, with a ground-state triplet multiplicity. Thus, it already has the appropriate electrostructural features to allow dimerisation through the boron atoms. Geometry scans along the B–B bond stretching mode reveal that, indeed, this dimerisation is barrierless (see Fig. S7†). In contrast, the NHC version of the cyclotetrameric structure, herein labelled as **NHC4cl**, is sterically crowded (see Fig. S8†). As a consequence, while the free energy of **4cl** is −39 kcal mol^{-1} relative to that of two **2-dib** species, the free energy of **NHC4cl** is +45 kcal mol^{-1} relative to that of two isolated ^{NHC}**2-dib** systems. These results strongly suggest that the formation of the diborene ^{NHC}**2-dib** from fleeting triplet borylenes is feasible, albeit less likely to happen than with singlet borylenes. These findings could pave the way for new synthetic methods for the formation of boron–boron multiply bonded systems, or alternatively non-dimerising systems for small-molecule activation, which will be explored in subsequent studies.

Conclusions

In summary, we apply DFT, natural bond orbital, natural resonance theory, and high-level multireference calculations to investigate the electronic, structural, bonding, and kinetic factors driving the spontaneous cyclotetramerisation of a CAAC-stabilised boron(I) species, and the reasons why its interconversion into a boron–boron doubly bonded compound through a Wanzlick-type equilibrium is hampered. In addition, we investigate why the NHC counterparts tend to dimerise, which is not the case for CAAC-stabilised boron(I) species. The cyanoborylene species **1**, which features a linear ^{CAAC}C–B–CN motif, strong B → ^{CAAC}C backdonation, and a closed-shell singlet multiplicity, preferably undergoes a barrierless dimerisation leading to a bis(borylene) compound through formation of a boron–nitrogen bond. Indeed, the diffusion-controlled, cascade oligomerisation of **1** following this route is not hampered by kinetic barriers, and the formation of the final reaction product is driven by diffusion-free cycloisomerisation steps. While high energy barriers are obtained for the cyclisation to six- and nine-membered $(BCN)_n$ rings from their corresponding open-chain isomers due to electronic and structural factors, the formation of the butterfly-type, cyclotetrameric twelve-membered ring **4cl** is both virtually barrierless and highly exergonic. In contrast, dimerisation of **1** through the boron atoms has a free-energy barrier of +11 kcal mol^{-1}, while the dissociation of the diborene **2-dib** to its monomeric units is uphill by +78 kcal mol^{-1}. Besides correctly predicting the reactivity of **1**, and hinting towards a synthetic route for elusive diborene-stabilised borylenes, our results provide thermodynamic and kinetic reasoning for the non-interconvertibility of **4cl** and **2-dib** and the lack of a Wanzlick-type equilibrium between **1** and **2-dib**. We also use computations to explore the reactivity of **4cl** and **2-dib** with Ph_2S_2, indicating that in both cases their deconstruction to a tetracoordinate boron(III) species is thermodynamically favourable. Finally, the replacement of the CAAC ligand to a classic NHC in the singly Lewis-base-stabilised species **1** leads to a triplet borylene featuring an ^{NHC}C–B–CN motif, whose electronic and structural properties allow its dimerisation through the boron atom. Additional computations for the corresponding [LHB:] parent borylenes indicate that the preference of CAACs for closed-shell singlet compounds, and those of conventional NHCs for triplet compounds, might be a general trend in borylene chemistry. Further studies aimed at investigating the generality of these findings, and at developing new synthetic avenues to boron–boron multiply bonded systems based on this approach, are underway in our laboratories.

© 2022 The Author(s). Published by the Royal Society of Chemistry

Open Access Article. Published on 04 March 2022. Downloaded on 2/6/2026 3:42:06 PM. This article is licensed under a Creative Commons Attribution-NonCommercial 3.0 Unported Licence.

Data availability

All relevant data is presented in the paper and ESI. The Cartesian coordinates of all computed structures are provided as part of the ESI.†

Author contributions

F. F. and B. E. designed the computations which were performed by F. F. and Y. J. F. F., B. E. and R. D. wrote the original draft. H. B., F. W. and B. E. acquisited fundings and contributed methodologies. All authors contributed to the interpretation of the computed data and the writing and editing of the manuscript.

Conflicts of interest

There are no conflicts to declare.

Acknowledgements

This project was funded by the European Research Council (ERC) under the European Union Horizon 2020 Research and Innovation Program (grant agreement no. 669054) and the Deutsche Forschungsgemeinschaft (DFG), *e.g.* in the framework of the GRK2112. F. F. thanks the Coordenação de Aperfeiçoamento de Pessoal de Nível Superior (CAPES) and the Alexander von Humboldt (AvH) Foundation for a Capes-Humboldt postdoctoral fellowship.

Notes and references

1 (*a*) H.-W. Wanzlick and H.-J. Kleiner, *Angew. Chem.*, 1961, **73**, 493; (*b*) H. W. Wanzlick, *Angew. Chem., Int. Ed. Engl.*, 1962, **1**, 75–80; (*c*) H.-W. Wanzlick, F. Esser and H.-J. Kleiner, *Chem. Ber.*, 1963, **96**, 1208–1212; (*d*) F. E. Hahn, L. Wittenbecher, D. Le Van and R. Fröhlich, *Angew. Chem., Int. Ed.*, 2000, **39**, 541–544; *Angew. Chem.*, 2000, **112**, 551–554; (*e*) V. P. W. Böhm and W. A. Herrmann, *Angew. Chem., Int. Ed.*, 2000, **39**, 4036–4038; *Angew. Chem.*, 2000, **112**, 4200–4202.

2 (*a*) D. Bourissou, O. Guerret, F. P. Gabbaï and G. Bertrand, *Chem. Rev.*, 2000, **100**, 39–92; (*b*) T. Dröge and F. Glorius, *Angew. Chem., Int. Ed.*, 2010, **49**, 6940–6952; *Angew. Chem.*, 2010, **122**, 7094–7107; (*c*) M. N. Hopkinson, C. Richter, M. Schedler and F. Glorius, *Nature*, 2014, **510**, 485–496.

3 S. Tsutsui, K. Sakamoto and M. Kira, *J. Am. Chem. Soc.*, 1998, **120**, 9955–9956.

4 R. Falconer, K. Byrne, G. Nichol, T. Krämer and M. Cowley, 2021, ChemRxiv, This content is a preprint and has not been peer-reviewed.

5 (*a*) M. Krasowska and H. F. Bettinger, *J. Am. Chem. Soc.*, 2012, **134**, 17094–17103; (*b*) F. Fantuzzi, T. M. Cardozo and M. A. C. Nascimento, *J. Phys. Chem. A*, 2015, **119**, 5335–5343; (*c*) M. Krasowska, M. Edelmann and H. F. Bettinger, *J. Phys. Chem. A*, 2016, **120**, 6332–6341.

6 D. Lu, Y. He and C. Wu, *Phys. Chem. Chem. Phys.*, 2019, **21**, 23533–23540.

7 F. Dahcheh, D. Martin, D. W. Stephan and G. Bertrand, *Angew. Chem., Int. Ed.*, 2014, **53**, 13159–13163; *Angew. Chem.*, 2014, **126**, 13375–13379.

8 A. D. Ledet and T. W. Hudnall, *Dalton Trans.*, 2016, **45**, 9820–9826.

9 H. Braunschweig, R. D. Dewhurst, F. Hupp, M. Nutz, K. Radacki, C. W. Tate, A. Vargas and Q. Ye, *Nature*, 2015, **522**, 327–330.

10 (*a*) H. Braunschweig, I. Krummenacher, M.-A. Légaré, A. Matler, K. Radacki and Q. Ye, *J. Am. Chem. Soc.*, 2017, **139**, 1802–1805; (*b*) C. Pranckevicius, M. Weber, I. Krummenacher, A. K. Phukan and H. Braunschweig, *Chem. Sci.*, 2020, **11**, 11055–11059.

11 (*a*) M.-A. Légaré, G. Bélanger-Chabot, R. D. Dewhurst, E. Welz, I. Krummenacher, B. Engels and H. Braunschweig, *Science*, 2018, **359**, 896–900; (*b*) M.-A. Légaré, M. Rang, G. Bélanger-Chabot, J. I. Schweizer, I. Krummenacher, R. Bertermann, M. Arrowsmith, M. C. Holthausen and H. Braunschweig, *Science*, 2019, **363**, 1329–1332; (*c*) M.-A. Légaré, G. Bélanger-Chabot, M. Rang, R. D. Dewhurst, I. Krummenacher, R. Bertermann and H. Braunschweig, *Nat. Chem.*, 2020, **12**, 1076–1080.

12 S. Hagspiel, M. Arrowsmith, F. Fantuzzi, A. Vargas, A. Rempel, A. Hermann, T. Brückner and H. Braunschweig, *Angew. Chem., Int. Ed.*, 2021, **60**, 6446–6450; *Angew. Chem.*, 2021, **133**, 6519–6524.

13 (*a*) R. Kinjo, B. Donnadieu, M. A. Celik, G. Frenking and G. Bertrand, *Science*, 2011, **333**, 610–613; (*b*) M. A. Celik, R. Sure, S. Klein, R. Kinjo, G. Bertrand and G. Frenking, *Chem.–Eur. J.*, 2012, **18**, 5676–5692; (*c*) D. A. Ruiz, M. Melaimi and G. Bertrand, *Chem. Commun.*, 2014, **50**, 7837–7839; (*d*) L. Kong, Y. Li, R. Ganguly, D. Vidovic and R. Kinjo, *Angew. Chem., Int. Ed.*, 2014, **53**, 9280–9283; *Angew. Chem.*, 2014, **126**, 9434–9437; (*e*) H. Wang, J. Zhang, Z. Lin and Z. Xie, *Chem. Commun.*, 2015, **51**, 16817–16820; (*f*) L. Kong, W. Lu, L. Yongxin, R. Ganguly and R. Kinjo, *Inorg. Chem.*, 2017, **56**, 5586–5593; (*g*) M. Arrowsmith, J. I. Schweizer, M. Heinz, M. Härterich, I. Krummenacher, M. C. Holthausen and H. Braunschweig, *Chem. Sci.*, 2019, **10**, 5095–5103; (*h*) U. Schmidt, F. Fantuzzi, M. Arrowsmith, A. Hermann, D. Prieschl, A. Rempel, B. Engels and H. Braunschweig, *Chem. Commun.*, 2020, **56**, 14809–14812.

14 (*a*) Y. Wang, B. Quillian, P. Wei, C. S. Wannere, Y. Xie, R. B. King, H. F. Schaefer, P. v. R. Schleyer and G. H. Robinson, *J. Am. Chem. Soc.*, 2007, **129**, 12412–12413; (*b*) Y. Wang, B. Quillian, P. Wei, Y. Xie, C. S. Wannere, R. B. King, H. F. Schaefer, P. v. R. Schleyer and G. H. Robinson, *J. Am. Chem. Soc.*, 2008, **130**, 3298–3299; (*c*) H. Braunschweig and R. D. Dewhurst, *Angew. Chem., Int. Ed.*, 2013, **52**, 3574–3583; *Angew. Chem.*, 2013, **125**, 3658–3667; (*d*) M. Arrowsmith, H. Braunschweig and T. E. Stennett, *Angew. Chem., Int. Ed.*, 2017, **56**, 96–115; *Angew. Chem.*, 2017, **129**, 100–120; (*e*) M.-A. Légaré, C. Pranckevicius and H. Braunschweig, *Chem. Rev.*, 2019, **119**, 8231–8261.

Open Access Article. Published on 04 March 2022. Downloaded on 2/6/2026 3:42:06 PM. This article is licensed under a Creative Commons Attribution-NonCommercial 3.0 Unported Licence.

15 (*a*) Y. Su and R. Kinjo, *Coord. Chem. Rev.*, 2017, **352**, 346–378; (*b*) S. Kundu, S. Sinhababu, V. Chandrasekhar and H. W. Roesky, *Chem. Sci.*, 2019, **10**, 4727–4741; (*c*) S. Hagspiel, M. Arrowsmith, F. Fantuzzi, A. Hermann, V. Paprocki, R. Drescher, I. Krummenacher and H. Braunschweig, *Chem. Sci.*, 2020, **11**, 551–555.

16 L. Wu, R. D. Dewhurst, H. Braunschweig and Z. Lin, *Organometallics*, 2021, **40**, 766–775.

17 (*a*) J. Böhnke, H. Braunschweig, T. Dellermann, W. C. Ewing, T. Kramer, I. Krummenacher and A. Vargas, *Angew. Chem., Int. Ed.*, 2015, **54**, 4469–4473; *Angew. Chem.*, 2015, **127**, 4551–4555; (*b*) M. Arrowsmith, D. Auerhammer, R. Bertermann, H. Braunschweig, G. Bringmann, M. A. Celik, R. D. Dewhurst, M. Finze, M. Grüne, M. Hailmann, T. Hertle and I. Krummenacher, *Angew. Chem., Int. Ed.*, 2016, **55**, 14464–14468; *Angew. Chem.*, 2016, **128**, 14680–14684; (*c*) D. Auerhammer, M. Arrowsmith, R. D. Dewhurst, T. Kupfer, J. Böhnke and H. Braunschweig, *Chem. Sci.*, 2018, **9**, 2252–2260.

18 F. Weinhold, C. R. Landis and E. D. Glendening, *Int. Rev. Phys. Chem.*, 2016, **35**, 399–440.

19 (*a*) C. Riplinger and F. Neese, *J. Chem. Phys.*, 2013, **138**, 034106; (*b*) C. Riplinger, B. Sandhoefer, A. Hansen and F. Neese, *J. Chem. Phys.*, 2013, **139**, 134101; (*c*) C. Riplinger, P. Pinski, U. Becker, E. F. Valeev and F. Neese, *J. Chem. Phys.*, 2016, **144**, 024109; (*d*) M. Saitow, U. Becker, C. Riplinger, E. F. Valeev and F. Neese, *J. Chem. Phys.*, 2017, **146**, 164105; (*e*) Y. Guo, C. Riplinger, U. Becker, D. G. Liakos, Y. Minenkov, L. Cavallo and F. Neese, *J. Chem. Phys.*, 2018, **148**, 011101.

20 (*a*) C. Angeli, R. Cimiraglia, S. Evangelisti, T. Leininger and J.-P. Malrieu, *J. Chem. Phys.*, 2001, **114**, 10252–10264; (*b*) C. Angeli, R. Cimiraglia and J.-P. Malrieu, *Chem. Phys. Lett.*, 2001, **350**, 297–305; (*c*) C. Angeli, R. Cimiraglia and J.-P. Malrieu, *J. Chem. Phys.*, 2002, **117**, 9138–9153.

21 (*a*) S. H. Vosko, L. Wilk and M. Nusair, *Can. J. Phys.*, 1980, **58**, 1200–1211; (*b*) C. Lee, W. Yang and R. G. Parr, *Phys. Rev. B: Condens. Matter Mater. Phys.*, 1988, **37**, 785–789; (*c*) A. D. Becke, *J. Chem. Phys.*, 1993, **98**, 5648–5652; (*d*) P. J. Stephens, F. J. Devlin, C. F. Chabalowski and M. J. Frisch, *J. Phys. Chem.*, 1994, **98**, 11623–11627.

22 (*a*) S. Grimme, J. Antony, S. Ehrlich and H. Krieg, *J. Chem. Phys.*, 2010, **132**, 154104; (*b*) S. Grimme, S. Ehrlich and L. Goerigk, *J. Comput. Chem.*, 2011, **32**, 1456–1465.

23 F. Weigend and R. Ahlrichs, *Phys. Chem. Chem. Phys.*, 2005, **7**, 3297–3305.

24 J.-D. Chai and M. Head-Gordon, *Phys. Chem. Chem. Phys.*, 2008, **10**, 6615.

25 K. Ishida, K. Morokuma and A. Komornicki, *J. Chem. Phys.*, 1977, **66**, 2153–2156.

26 A. V. Marenich, C. J. Cramer and D. G. Truhlar, *J. Phys. Chem. B*, 2009, **113**, 6378–6396.

27 (*a*) C. P. Kelly, C. J. Cramer and D. G. Truhlar, *J. Chem. Theory Comput.*, 2005, **1**, 1133–1152; (*b*) M. Sparta, C. Riplinger and F. Neese, *J. Chem. Theory Comput.*, 2014, **10**, 1099–1108; (*c*) F. Fantuzzi, M. A. C. Nascimento, B. Ginovska, R. M. Bullock and S. Raugei, *Dalton Trans.*, 2021, **50**, 840–849.

28 B. O. Roos, in *Advances in Chemical Physics: Ab Initio Methods in Quantum Chemistry Part 2, Volume 69*, ed. K. P. Lawley, John Wiley & Sons, 1987, pp. 399–445.

29 (*a*) E. Welz, J. Böhnke, R. D. Dewhurst, H. Braunschweig and B. Engels, *J. Am. Chem. Soc.*, 2018, **140**, 12580–12591; (*b*) S. K. Mellerup, Y. Cui, F. Fantuzzi, P. Schmid, J. T. Goettel, G. Bélanger-Chabot, M. Arrowsmith, I. Krummenacher, Q. Ye, V. Engel, B. Engels and H. Braunschweig, *J. Am. Chem. Soc.*, 2019, **141**, 16954–16960; (*c*) T. Thiess, G. Bélanger-Chabot, F. Fantuzzi, M. Michel, M. Ernst, B. Engels and H. Braunschweig, *Angew. Chem., Int. Ed.*, 2020, **59**, 15480–15486; *Angew. Chem.*, 2020, **132**, 15608–15614; (*d*) C. Saalfrank, F. Fantuzzi, T. Kupfer, B. Ritschel, K. Hammond, I. Krummenacher, R. Bertermann, R. Wirthensohn, M. Finze, P. Schmid, V. Engel, B. Engels and H. Braunschweig, *Angew. Chem., Int. Ed.*, 2020, **59**, 19338–19343; *Angew. Chem.*, 2020, **132**, 19502–19507; (*e*) T. Ullrich, P. Pinter, J. Messelberger, P. Haines, R. Kaur, M. M. Hansmann, D. Munz and D. M. Guldi, *Angew. Chem., Int. Ed.*, 2020, **59**, 7906–7914; *Angew. Chem.*, 2020, **132**, 7980–7988; (*f*) M. Pinheiro, F. B. C. Machado, F. Plasser, A. J. A. Aquino and H. Lischka, *J. Mater. Chem. C*, 2020, **8**, 7793–7804; (*g*) M. Rang, F. Fantuzzi, M. Arrowsmith, I. Krummenacher, E. Beck, R. Witte, A. Matler, A. Rempel, T. Bischof, K. Radacki, B. Engels and H. Braunschweig, *Angew. Chem., Int. Ed.*, 2021, **60**, 2963–2968; *Angew. Chem.*, 2021, **133**, 3000–3005; (*h*) D. K. Roy, T. Tröster, F. Fantuzzi, R. D. Dewhurst, C. Lenczyk, K. Radacki, C. Pranckevicius, B. Engels and H. Braunschweig, *Angew. Chem., Int. Ed.*, 2021, **60**, 3812–3819; *Angew. Chem.*, 2021, **133**, 3856–3863; (*i*) P. Schmid, F. Fantuzzi, J. Klopf, N. B. Schröder, R. D. Dewhurst, H. Braunschweig, V. Engel and B. Engels, *Chem.–Eur. J.*, 2021, **27**, 5160–5170; (*j*) M. K. Sharma, F. Ebeler, T. Glodde, B. Neumann, H.-G. Stammler and R. S. Ghadwal, *J. Am. Chem. Soc.*, 2021, **143**, 121–125; (*k*) M. K. Sharma, D. Rottschäfer, T. Glodde, B. Neumann, H. Stammler and R. S. Ghadwal, *Angew. Chem., Int. Ed.*, 2021, **60**, 6414–6418; *Angew. Chem.*, 2021, **133**, 6485–6489; (*l*) M. Gerlach, F. Fantuzzi, L. Wohlfart, K. Kopp, B. Engels, J. Bozek, C. Nicolas, D. Mayer, M. Gühr, F. Holzmeier and I. Fischer, *J. Chem. Phys.*, 2021, **154**, 114302; (*m*) A. Maiti, F. Zhang, I. Krummenacher, M. Bhattacharyya, S. Mehta, M. Moos, C. Lambert, B. Engels, A. Mondal, H. Braunschweig, P. Ravat and A. Jana, *J. Am. Chem. Soc.*, 2021, **143**, 3687–3692; (*n*) T. Brückner, F. Fantuzzi, T. E. Stennett, I. Krummenacher, R. D. Dewhurst, B. Engels and H. Braunschweig, *Angew. Chem., Int. Ed.*, 2021, **60**, 13661–13665; *Angew. Chem.*, 2021, **133**, 13774–13779; (*o*) M. Härterich, B. Ritschel, M. Arrowsmith, J. Böhnke, I. Krummenacher, A. K. Phukan and H. Braunschweig, *J. Am. Chem. Soc.*, 2021, **143**(43), 18339–18345.

30 (*a*) K. Yamaguchi, *Chem. Phys. Lett.*, 1975, **33**, 330–335; (*b*) S. Yamanaka, M. Okumura, M. Nakano and K. Yamaguchi,

© 2022 The Author(s). Published by the Royal Society of Chemistry

Open Access Article. Published on 04 March 2022. Downloaded on 2/6/2026 3:42:06 PM.
This article is licensed under a Creative Commons Attribution-NonCommercial 3.0 Unported Licence.

J. Mol. Struct., 1994, **310**, 205–218; (*c*) M. Nakano, *Top. Curr. Chem.*, 2017, **375**, 47.

31 (*a*) E. D. Glendening and F. Weinhold, *J. Comput. Chem.*, 1998, **19**, 593–609; (*b*) E. D. Glendening and F. Weinhold, *J. Comput. Chem.*, 1998, **19**, 610–627; (*c*) E. D. Glendening, J. K. Badenhoop and F. Weinhold, *J. Comput. Chem.*, 1998, **19**, 628–646.

32 M. J. Frisch, G. W. Trucks, H. B. Schlegel, G. E. Scuseria, M. A. Robb, J. R. Cheeseman, G. Scalmani, V. Barone, B. Mennucci, G. A. Petersson, H. Nakatsuji, M. Caricato, X. Li, H. P. Hratchian, A. F. Izmaylov, J. Bloino, G. Zheng, J. L. Sonnenberg, M. Hada, M. Ehara, K. Toyota, R. Fukuda, J. Hasegawa, M. Ishida, T. Nakajima, Y. Honda, O. Kitao, H. Nakai, T. Vreven, J. A. Montgomery Jr, J. E. Peralta, F. Ogliaro, M. Bearpark, J. J. Heyd, E. Brothers, K. N. Kudin, V. N. Staroverov, R. Kobayashi, J. Normand, K. Raghavachari, A. Rendell, J. C. Burant, S. S. Iyengar, J. Tomasi, M. Cossi, N. Rega, J. M. Millam, M. Klene, J. E. Knox, J. B. Cross, V. Bakken, C. Adamo, J. Jaramillo, R. Gomperts, R. E. Stratmann, O. Yazyev, A. J. Austin, R. Cammi, C. Pomelli, J. W. Ochterski, R. L. Martin, K. Morokuma, V. G. Zakrzewski, G. A. Voth, P. Salvador, J. J. Dannenberg, S. Dapprich, A. D. Daniels, Ö. Farkas, J. B. Foresman, J. V Ortiz, J. Cioslowski and D. J. Fox, *Gaussian 16, Revision C.01*, Gaussian, Inc., Wallingford CT, 2016.

33 F. Neese, *Wiley Interdiscip. Rev.: Comput. Mol. Sci.*, 2012, **2**, 73–78.

34 E. D. Glendening, C. R. Landis and F. Weinhold, *J. Comput. Chem.*, 2019, **40**, 2234–2241.

35 C. Y. Legault, *CYLview, version 1.0.561b. Université de Sherbrooke*, Sherbrooke, QC, Canada, 2009, http://www.cylview.org.

36 J. Böhnke, H. Braunschweig, W. C. Ewing, C. Hörl, T. Kramer, I. Krummenacher, J. Mies and A. Vargas, *Angew. Chem., Int. Ed.*, 2014, **53**, 9082–9085; *Angew. Chem.*, 2014, **126**, 9228–9231.

37 M. P. Mitoraj, A. Michalak and T. Ziegler, *J. Chem. Theory Comput.*, 2009, **5**, 962–975.

38 (*a*) M. Ernzerhof and G. E. Scuseria, *J. Chem. Phys.*, 1999, **110**, 5029–5036; (*b*) C. Adamo and V. Barone, *J. Chem. Phys.*, 1999, **110**, 6158–6170.

39 G. te Velde, F. M. Bickelhaupt, E. J. Baerends, C. Fonseca Guerra, S. J. A. van Gisbergen, J. G. Snijders and T. Ziegler, *J. Comput. Chem.*, 2001, **22**, 931–967.

© 2022 The Author(s). Published by the Royal Society of Chemistry